Paper

Int'l J. of Aeronautical & Space Sci. 16(3), 475–483 (2015)
DOI: http://dx.doi.org/10.5139/IJASS.2015.16.3.475

IJASS
International Journal of Aeronautical and Space Sciences

Simulation of Dynamic EADs Jamming Performance against Tracking Radar in Presence of Airborne Platform

Jae-Won Rim*, Ki-Hwan Jung and Il-Suek Koh*****

Department of Electronics Engineering, Inha University, Incheon 22212, Korea

Chung Baek** and Seungsoo Lee*******

Department of Aerospace Engineering, Inha University, Incheon 22212, Korea

Seung-Ho Choi*****

Agency for Defense Development, Daejeon 34188, Korea

Abstract

We propose a numerical scheme to simulate the time-domain echo signals at tracking radar for a realistic scenario where an EAD (expendable active decoy) and an airborne target are both in dynamic states. On various scenarios where the target takes different maneuvers, the trajectories of the EAD ejected from the target are accurately calculated by solving 6-DOF (Degree-of-Freedom) equations of the motion for the EAD. At each sampling time of the echo signal, the locations of the EAD and the target are assumed to be fixed. Thus, the echo power from the EAD can be simply calculated by using the Friis transmission formula. The returned power from the target can be computed based on the pre-calculated scattering matrix of the target. In this paper, an IPO (iterative physical optics) method is used to construct the scattering matrix database of the target. The sinc function-interpolation formulation (sampling theorem) is applied to compute the scattering at any incidence angle from the database. A simulator is developed based on the proposed scheme to estimate the echo signals, which can consider the movement of the airborne target and EAD, also the scattering of the target and the RF specifications of the EAD. For applications, we consider the detection probability of the target in the presence of the EAD based on Monte Carlo simulation.

Key words: EAD, Radar jamming, 6-DOF

1. Introduction

ECM (electronic countermeasures) technology has progressively become more specialized and sophisticated during the last half century [1]. Among a large number of ECM technologies, the active decoy has been one of effective means to deceive and threaten tracking radar as this type of decoy has advantages of low cost and high jamming performance [2]. In recent years, a few researches about a TRAD (towed radar active decoy) have been reported [3-5]. The research about the TRAD has mainly concentrated on the jamming principle or the analysis of the jamming performance [4, 5]. However, there are few literatures about the EAD (expendable active decoy). One of the advantages of the EAD is that it can be an effective mean to counteract the mono-pulse RF seeker [6]. The design of a high-performance EAD for an effective deception against the tracking radar and RF seeker strongly depends on the operation scenario. Different scenarios will require different design parameters of the EAD, where the airborne platform, the EAD, and the tracking radar(RF seeker) operate independently. Hence, an accurate simulation method to measure the jamming performance of the EAD is essential, which requires calculating the echo signals from the target and the EAD for

* MD Student
** Ph. D Student
*** Professor, Corresponding author: ikoh@inha.ac.kr
**** Ph. D Student
***** Professor
****** Principal Researcher

Received: June 30, 2015 Revised: August 25, 2015 Accepted: August 31, 2015

http://ijass.org pISSN: 2093-274x eISSN: 2093-2480

various scenarios such as the movement of the target and EAD, as well as various RF specifications of the EAD and the tracking radar. In the light of optimally designing EAD for the effective jamming performance, RF design parameters such as antenna gain, antenna beam pattern, polarization, and internal power amplifier gain should be considered. In this work, thus, we calculate the probability of missing target depending on different beam patterns, polarization and power amp gain to evaluate the jamming performance of the EAD.

In this paper, we propose a scheme to simulate the echo signals at the tracking radar based on specific operation scenarios of the EAD and tracking radar. In section 2, a considered scenario is addressed where the operations of the tracking radar, the EAD, and the target are described. The simulation models for the EAD and tracking radar are also provided. And we formulate the echo signals from the EAD and target based on the Friis transmission formula. Then, the tracking mode of the tracking radar is explained. Finally, some simulation results are addressed on three different scenarios for two EAD designs in section 3.

2. Calculation of echo signals at tracking radar

Figure 1 shows a deployment scenario considered in this paper: while a target moves along an arbitrary path with a specific velocity, tracking radar may detect and start to track the target if the target comes within the maximum detection range of the radar. To avoid being tracked, the target ejects an EAD to try to deceive the radar, which can allow the target to evade from the radar detection. To estimate how effectively the EAD deceives the radar, a simulation method is required calculating two echo signals at the radar location in time domain: the jamming signal from the EAD and the scattered signal by the target. In

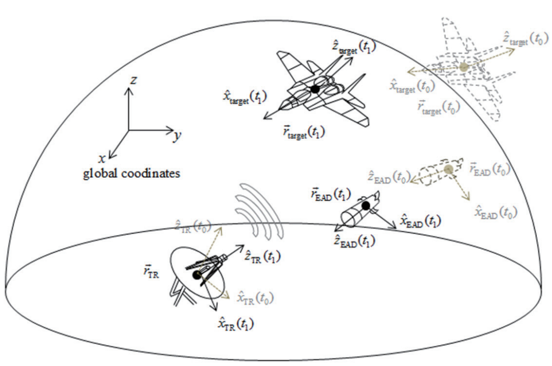

Fig. 1. Deployment scenario of EAD in the presence of target and tracking radar.

this paper, the repeater-type EAD is considered, which amplifies the received signal from the radar and then re-transmits it back to the radar. Hence, the EAD can be modeled by a simple RF system consisting of an antenna and a power amplifier. The tracking radar can be modeled with a moving antenna beam. The scattered signal from the target can be computed based on the pre-calculated scattering matrices. In this paper, it is assumed that there is no ground plane effect. All computed quantities should be a function of time to consider the movement of the EAD, target, and the tracking antenna beam. The radar transmits a signal at every PRI (pulse repetition interval). In each PRI, the movement of the EAD and the target is negligible. Thus, in each PRI, we can calculate the echo signals from the target and the EAD by assuming that their locations are fixed. All required information is originally defined in the local coordinates for the EAD, the target, and the tracking radar, including the antenna pattern and the polarization of the tracking radar and the EAD, and the scattering matrix of the target, which are summarized as

$\vec{r}_{\text{target}}, \vec{r}_{\text{EAD}}, \vec{r}_{\text{TR}}$	Locations of target, EAD, and tracking radar in global coordinates
$\hat{x}_{\text{target}}, \hat{y}_{\text{target}}, \hat{z}_{\text{target}}$	Local coordinate system of target in global coordinates
$\hat{x}_{\text{EAD}}, \hat{y}_{\text{EAD}}, \hat{z}_{\text{EAD}}$	Local coordinate system of EAD in global coordinates
$\hat{x}_{\text{target}}, \hat{y}_{\text{target}}, \hat{z}_{\text{target}}$	Local coordinate system of tracking radar in global coordinates
$\hat{x}_{\text{TR}}, \hat{y}_{\text{TR}}, \hat{z}_{\text{TR}}$	Unit propagation vectors from tracking radar to target and to EAD in local coordinates of tracking radar
$\hat{k}^{i}_{\text{TR}\to\text{target}}, \hat{k}^{i}_{\text{TR}\to\text{EAD}}$	Unit propagation vector from tracking radar to EAD in local coordinates of EAD
$\hat{k}^{i}_{l,\text{EAD}}$	Unit propagation vector from tracking radar to target in local coordinates of target
k_0	Free-space propagation constant
λ	Wavelength
P_{trans}	Transmitted power by tracking radar
$G_{\text{TR}}, G_{\text{EAD}}$	Antenna gains of tracking radar and EAD, respectively
G_{amp}	Gain of internal amplifier of EAD
$\hat{\rho}_{\text{TR}}, \hat{\rho}_{\text{EAD}}$	Unit polarization vectors of tracking radar and EAD in local coordinates
$R_{\text{TR}\to\text{t}}$	Distance between tracking radar and target
$R_{\text{TR}\to\text{d}}$	Distance between tracking radar and EAD

2.1 Prediction of Trajectories of EAD

In order to assess the effectiveness of decoy, it is crucial to predict the trajectories of the EAD after it is released from the mother aircraft (target). In this paper, a program that can predict the trajectories of the EAD ejected from the target has been developed. It solves the 6-DOF equations of motion for the EAD. The aerodynamic forces and moments of the EAD during the separation are influenced by the presence of the target. This interference effect is modeled via so-called interference database of the target. The fundamental assumption behind the validity of the interference database is that the interference effect of the EAD aerodynamics is far stronger than that of the target. The interference flow field is constructed with CFD (Computational Fluid Dynamics) analysis of the EAD under the influence of the target. The detailed analysis method can be found in [7]. The trajectories of the EAD depend on the scenario of the release: time of separation, target maneuver, ejector force and so on. In this paper, the target is selected as F-15 aircraft. Table 1 shows the physical specifications of the target and the EAD.

2.2 Coordinate transformation matrix

As the local incidence angle of the incident signal on the EAD and the target varies during every PRI as shown in Fig. 1, the coordinate transformation matrices are essential to convert the global coordinates into the local coordinates and vice versa. The coordinate transformation matrices, $\bar{\bar{T}}_{l\to g}$ and $\bar{\bar{T}}_{g\to l}$ can be defined as

$$\bar{\bar{T}}_{l\to g} = \left[\hat{x}_g(t)^T : \hat{y}_g(t)^T : \hat{z}_g(t)^T\right],\ \bar{\bar{T}}_{g\to l} = \bar{\bar{T}}_{l\to g}^{\,-1} = \bar{\bar{T}}_{l\to g}^{\,T}, \quad (1)$$

where the subscriptions, g and l denote the global and local coordinates, respectively. A unit vector in global coordinates, $\hat{v}_g(t)$ can be converted into local coordinates by $\hat{v}_l^T(t) = \bar{\bar{T}}_{g\to l} \cdot \hat{v}_g^{\,T}(t)$ where superscript T denotes the matrix transpose.

Figure 2 shows the local coordinates of the tracking radar, EAD, and target. The azimuth and elevation angles of the incidence waves in their local spherical coordinates can be computed as

$$\hat{k}^i_{\mathrm{TR}\to\mathrm{target}}:\ \theta_{l,\mathrm{TR}\to\mathrm{t}}(t) = \cos^{-1}\left(\hat{z}_{l,\mathrm{TR}} \cdot \hat{k}^i_{\mathrm{TR}\to\mathrm{target}}(t)\right),$$
$$\phi_{l,\mathrm{TR}\to\mathrm{t}}(t) = \cos^{-1}\left(\frac{\hat{k}^i_{\mathrm{TR}\to\mathrm{target}}(t)\cdot\hat{y}_{l,\mathrm{TR}}}{\sin\theta_{l,\mathrm{TR}\to\mathrm{t}}(t)}\right) \quad (2)$$

$$\hat{k}^i_{\mathrm{TR}\to\mathrm{EAD}}:\ \theta_{l,\mathrm{TR}\to\mathrm{d}}(t) = \cos^{-1}\left(\hat{z}_{l,\mathrm{TR}} \cdot \hat{k}^i_{\mathrm{TR}\to\mathrm{EAD}}(t)\right),$$
$$\phi_{l,\mathrm{TR}\to\mathrm{d}}(t) = \cos^{-1}\left(\frac{\hat{k}^i_{\mathrm{TR}\to\mathrm{EAD}}(t)\cdot\hat{y}_{l,\mathrm{TR}}}{\sin\theta_{l,\mathrm{TR}\to\mathrm{d}}(t)}\right) \quad (3)$$

$$\hat{k}^i_{l,\mathrm{EAD}}:\ \theta_{l,\mathrm{EAD}}(t) = \cos^{-1}\left(-\hat{z}_{l,\mathrm{EAD}} \cdot \hat{k}^i_{l,\mathrm{EAD}}(t)\right),$$
$$\phi_{l,\mathrm{EAD}}(t) = \cos^{-1}\left(-\frac{\hat{k}^i_{l,\mathrm{EAD}}(t)\cdot\hat{y}_{l,\mathrm{EAD}}}{\sin\theta_{l,\mathrm{EAD}}(t)}\right) \quad (4)$$

Table 1. Physical specifications of target and EAD

	Target (F15)		EAD
Weight [kg]	20200	Weight [kg]	2.8
MAC [m]	4.86	Diameter [mm]	5.5
Span [m]	13	Length [mm]	170
Ref. Area $[\mathrm{m}^2]$	56.5	C.G. location	(-40, 0, 0)
Ejection location	(-12, 1.5, 0.05)	M.O.I. $[kg\cdot\mathrm{m}^2]$	$\begin{bmatrix} 0.005 & 0 & 0 \\ 0 & 0.089 & 0 \\ 0 & 0 & 0.089 \end{bmatrix}$

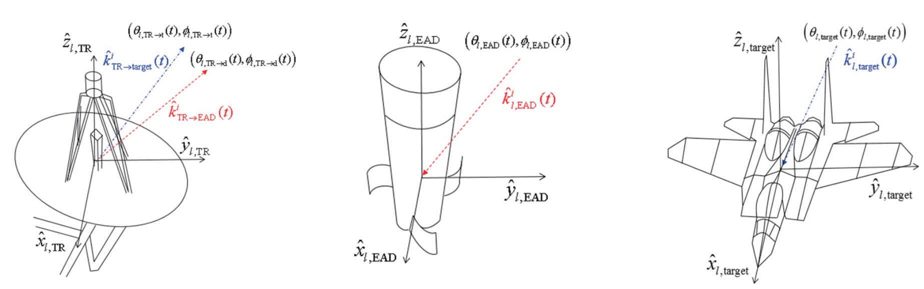

(a) (b) (c)

Fig. 2. Local coordinate systems. (a) Tracking radar, (b) EAD, and (c) Target.

$$\hat{k}^i_{l,\text{target}}:\ \theta_{l,\text{target}}(t)=\cos^{-1}\left(-\hat{z}_{l,\text{target}}\cdot\hat{k}^i_{l,\text{target}}(t)\right),$$
$$\phi_{l,\text{target}}(t)=\cos^{-1}\left(-\frac{\hat{k}^i_{l,\text{target}}(t)\cdot\hat{y}_{l,\text{target}}}{\sin\theta_{l,\text{target}}(t)}\right) \tag{5}$$

2.3 Scattering matrices of target and its interpolation

The scattering property of the target depends on the incidence angle of the incident wave on the target. To calculate the scattered power from the target, the scattering matrix is required at every incidence angle. Fig. 2 (c) shows the target geometry. In this paper, to calculate the scattering matrix of the target, we use the IPO method since it is a fast and accurate numerical method. The IPO repeatedly applies the PO (physical optics) method, so that it can partially consider multiple scattering among the target surface and can compensate the major weakness of the PO method [8 - 10]. Table 2 summarizes the overall dimension of the target. The monostatic scattering is calculated at every incidence angle at 2GHz.

Using the IPO method, the four scattering matrices, S_{hh}, S_{hv}, S_{vh} and S_{vv} can be computed where the subscripts h and v indicate the horizontal and vertical polarizations, respectively. Due to the reciprocity, S_{hv}=S_{vh}, so that three matrices are shown in Fig. 3.

Due to the arbitrary motion of the target, the radar signal can be incident on the target at arbitrary incidence angle. To accurately estimate scattering based on the pre-calculated scattering matrices, an interpolation scheme is required. We use a sinc-function interpolation scheme known as sampling theorem [11] and can efficiently retrieves the scattering

Table 2. Specification of target geometry for scattering analysis

Surface material	PEC (Perfect electric conductor)
Number of meshes	50278
Size of meshes	$\approx 1\lambda$
Maximum length of y-axis	$\approx 13m$
Maximum length of x-axis	$\approx 18m$

matrix values with a small amount of sampled data [12]. The sinc-function interpolation can be represented as

$$f(\theta,\phi)=\sum_{m=-m_{\max}}^{2m_{\max}}\sum_{n=-n_{\max}}^{2n_{\max}} f(\theta_m,\phi_n)\cdot\text{sinc}\left(\frac{\theta-m\Delta\theta}{\Delta\theta}\pi\right)\cdot\text{sinc}\left(\frac{\phi-n\Delta\phi}{\Delta\phi}\pi\right), \tag{6}$$

where $\Delta\theta$ and $\Delta\phi$ are the sampling intervals of the elevation and the azimuth angles, respectively. $f(\theta_m, \phi_m)$ is the sampled scattering data at the incidence angle, (θ_m, ϕ_m). sinc(x) is the sinc function, defined as $\sin(x)/x$ [12]. m_{max} and n_{max} are the sampling numbers for the elevation and the azimuth angles, respectively. The Nyquist condition should be satisfied to guarantee exact retrieval as

$$\Delta\theta(\text{or }\Delta\phi)\le\frac{\lambda}{2d}=\frac{\pi}{k_0 a}, \tag{7}$$

where$_a$ is the maximum dimension of the target. For the considered target, $\Delta\theta$(or $\Delta\phi$)≤0.0042° is required, which is not easy to be satisfied.

2.4 Echo signals from target and EAD

In the global coordinates shown in Fig. 1, the incident electric field from the tracking radar on the target is represented by using the Friis transmission formula [13] as

$$\vec{E}_g^{\,i}(t)=\sqrt{P_{\text{trans}}\cdot G_{\text{TR}}\left(\theta_{l,\text{TR}\to\text{t}}(t),\phi_{l,\text{TR}\to\text{t}}(t)\right)}\cdot\frac{e^{jk_0R_{\text{TR}\to\text{t}}(t)}}{4\pi R_{\text{TR}\to\text{t}}(t)}\hat{\rho}_{\text{TR}}(t), \tag{8}$$

where $\theta_{l,\text{TR}\to\text{t}}(t)$ and $\phi_{l,\text{TR}\to\text{t}}(t)$ can be computed by eq. (2). The incident field is converted into that in the local coordinates for the target by using eq. (1). In the local coordinates of the target, the horizontal and vertical polarizations for incident wave are defined as

$$\hat{h}_l^{\,i}(t)=\frac{\hat{k}^i_{l,\text{target}}(t)\times\hat{z}_{l,\text{target}}(t)}{\left|\hat{k}^i_{l,\text{target}}(t)\times\hat{z}_{l,\text{target}}(t)\right|},\ \hat{v}_l^{\,i}(t)=\hat{h}_l^{\,i}(t)\times\hat{k}^i_{l,\text{target}}(t). \tag{9}$$

After decomposing the incident wave into two locally polarized incident waves, the scattered wave by the target in its local coordinates can be computed based on the pre-

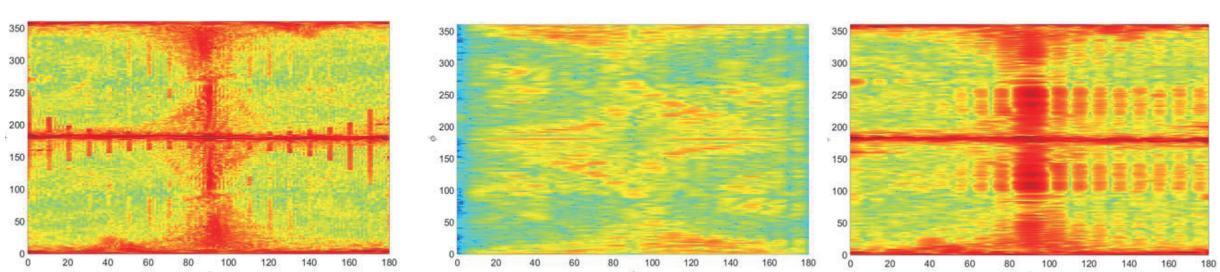

(a) (b) (c)

Fig. 3. 2D scattering matrix with respect to elevation and azimuth angles. (a) S_{hh}, (b) S_{hv}, and (c) S_{vv}.

DOI: http://dx.doi.org/10.5139/IJASS.2015.16.3.475

calculated scattering matrix. For the scattered wave, the propagation vector is opposite direction to the incident propagation vector $\hat{k}^{i}_{l,\text{target}}$. Thus, h-pol is opposite direction to $\hat{h}^{i}_{l}$ and v-pol is same direction with $\hat{v}^{i}_{l}$. Therefore, the scattered wave by the target in its local coordinates is expressed as

$$\begin{aligned}\vec{E}_l^{\,s}(t) &= \vec{E}_{h,l}^{\,s}(t)+\vec{E}_{v,l}^{\,s}(t)\\ &\sim \begin{bmatrix} -S_{hh}(\theta_{l,\text{target}}(t),\phi_{l,\text{target}}(t))\cdot\left(\vec{E}_l^{\,i}(t)\cdot\hat{h}_l^{i}(t)\right)\cdot\hat{h}_l^{i}(t)-S_{hv}(\theta_{l,\text{target}}(t),\phi_{l,\text{target}}(t))\cdot\left(\vec{E}_l^{\,i}(t)\cdot\hat{v}_l^{i}(t)\right)\cdot\hat{h}_l^{i}(t)\\ +S_{vh}(\theta_{l,\text{target}}(t),\phi_{l,\text{target}}(t))\cdot\left(\vec{E}_l^{\,i}(t)\cdot\hat{h}_l^{i}(t)\right)\cdot\hat{v}_l^{i}(t)+S_{vv}(\theta_{l,\text{target}}(t),\phi_{l,\text{target}}(t))\cdot\left(\vec{E}_l^{\,i}(t)\cdot\hat{v}_l^{i}(t)\right)\cdot\hat{v}_l^{i}(t)\end{bmatrix}\end{aligned} \quad (10)$$

where $\vec{E}_l^{\,i}(t)$ is the incident field in the local coordinates of the target, and $\theta_{l,\text{target}}(t)$ and $\phi_{l,\text{target}}(t)$ can be computed by using eq. (5). By converting the scattered field into that in the global coordinates using eq. (1) and applying the Friis transmission formula again, the received echo signal at the tracking radar is expressed as

$$\vec{\sigma}_{\text{scattered}}(t)=\sqrt{G_{\text{TR}}\left(\theta_{l,\text{TR}\to\text{t}}(t),\phi_{l,\text{TR}\to\text{t}}(t)\right)}\cdot\frac{\lambda}{4\pi}\cdot\frac{e^{jk_0R_{\text{TR}\to\text{t}}(t)}}{R_{\text{TR}\to\text{t}}(t)}\cdot\left(\overline{\overline{T}}_{l\to g}^{\,\text{target}}\cdot\vec{E}_l^{\,s}(t)\right) \quad (11)$$

The next procedure is the method to compute the echo signal from the EAD. The received power at the EAD from the tracking radar can be calculated as

$$\begin{aligned}P_{\text{Rx by EAD}}(t)&=P_{\text{trans}}\cdot G_{\text{TR}}\left(\theta_{l,\text{TR}\to\text{d}}(t),\phi_{l,\text{TR}\to\text{d}}(t)\right)\cdot G_{\text{EAD}}\left(\theta_{l,\text{EAD}}(t),\phi_{l,\text{EAD}}(t)\right)\\ &\cdot\left(\frac{\lambda}{4\pi R_{\text{TR}\to\text{d}}(t)}\right)^2\cdot\left|\hat{\rho}_{\text{TR}}(t)\cdot\hat{\rho}_{\text{EAD}}(t)\right|^2\end{aligned} \quad (12)$$

where $\theta_{l,\text{TR}\to\text{d}}(t)$ and $\phi_{l,\text{TR}\to\text{d}}(t)$ can be computed by eq. (3). $\theta_{l,\text{EAD}}(t)$ and $\phi_{l,\text{EAD}}(t)$ are obtained by eq. (4). $\left|\hat{\rho}_{\text{TR}}(t)\cdot\hat{\rho}_{\text{EAD}}(t)\right|^2$ denotes the polarization loss factor [13]. The received power at the EAD is amplified by its internal RF system to maximize the jamming. Hence, the transmitted power becomes $P_{\text{Tx by EAD}}(t)=G_{\text{amp}}\cdot P_{\text{Rx by EAD}}(t)$. By applying the Friis transmission formula again, finally, the jamming signal from the EAD at the tracking radar can be calculated by

$$\begin{aligned}\vec{\sigma}_{\text{Jamming}}(t)&=\sqrt{P_{\text{Tx by EAD}}(t)\cdot G_{\text{TR}}\left(\theta_{l,\text{TR}\to\text{d}}(t),\phi_{l,\text{TR}\to\text{d}}(t)\right)\cdot G_{\text{EAD}}\left(\theta_{l,\text{EAD}}(t),\phi_{l,\text{EAD}}(t)\right)}\\ &\cdot\left(\frac{\lambda}{4\pi}\right)\cdot\frac{e^{jk_0R_{\text{TR}\to\text{d}}(t)}}{R_{\text{TR}\to\text{d}}(t)}\cdot\hat{\rho}_{\text{EAD}}(t)\end{aligned} \quad (13)$$

(11) and (13) are added into the total echo signal from the target and the EAD with considering polarization vector of the tracking radar as

$$P_{\text{total}}(t)=\left|\left(\vec{\sigma}_{\text{scattered}}(t)+\vec{\sigma}_{\text{Jamming}}(t)\right)\cdot\hat{\rho}_{\text{TR}}(t)\right|^2 \quad (14)$$

2.5 Scanning and Tracking modes

We adopt the scanning and tracking modes: the circular scanning mode that monitors a large area to detect a target and the conical scanning mode that keeps tracking the target when the target is detected in the circular scanning mode [14].

Figure 4 shows a typical conical scan operation. As the beam revolves around the LOS (line-of-sight) axis with a certain squint angle, the radar measures the returned signals during one scan [15]. Here, the squint angle is assumed as 1.5°. After scanning, the tracking radar determines the direction in which the antenna must be moved by comparing power difference and continues scanning and tracking sequentially. Fig. 5 shows the basic tracking flow chart. The scenario adopted in this paper is as follows: the tracking radar keeps searching a large area in the circular scanning mode with a broad HPBW antenna beam. After the radar searches over the whole azimuth 360° at elevation 45° by the circular scan, it determines the azimuth angle by comparing the peak power with the detection threshold. It also determines the elevation angle by sweeping the beam in the elevation direction at the azimuth angle where the peak power occurs above the detection threshold. If the azimuth and elevation angles are estimated by the circular scanning mode, it converts its mode into the conical scanning mode for the precise arrival angle estimation with a narrow pencil beam. Here, the HPBW (Half Power Beam Width) is 30° for the circular scan and 3° for the conical scan. And the scan rates are assumed as 2 [rotations/s] for the circular scan and 4 [rotations/s] for the conical scan, respectively [15].

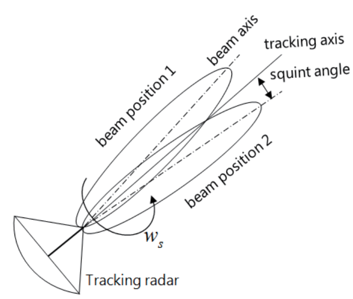

Fig. 4. Conical scan operation.

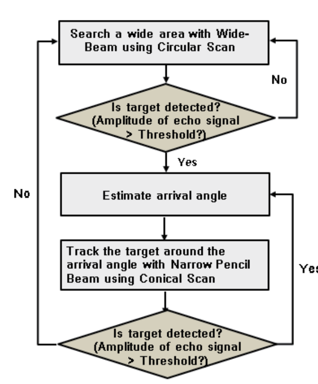

Fig. 5. Basic tracking flow chart.

3. Simulation

First, we verify the simulation code by considering a specific scenario where the scattered power from the target can be analytically calculated by using the radar range equation [13]. The tracking radar is fixed at the origin and transmits the *x*-directed polarized wave, $\hat{\rho}_{TR} = \hat{x}_{TR} = [1,0,0]$ whose transmission power is assumed as1 kW. The target is fixed at (0, 5000, 0) and rotates 360º around its local z-axis, $\hat{z}_{target}(0) = [0,\ -\sqrt{3}/2,\ 1/2]$ for 18 seconds. The received power is computed every 0.01 s. For this scenario, the movement of the target is not considered and the gain of the tracking radar is assumed as 1 for simplicity of calculation. As the incident angle on the target is constant, 30º in the local coordinates, the reflected power from the target can be easily calculated using the radar range equation. Fig. 6 shows the comparison of the results of eqs. (8) - (11), and the analytical calculation, which are in exact agreement.

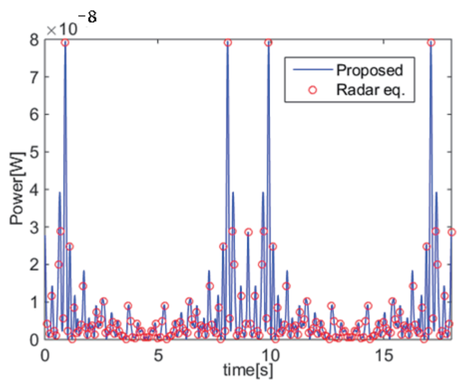

Fig. 6. Comparison of echo powers from fixed target.

For the rest simulation, we consider two different beam patterns of the EAD, in which one pattern has 90º degrees HPBW with the gain of 5.942(End-fire) and the other has broader beam pattern with the gain of 1.27(broad-side) as shown in Fig. 7.

Also, we consider three different operation scenarios shown in Table 3.

On all the scenarios, the initial location of the target in the global coordinates is given as $\vec{r}_{target}(0) = (0,-5000,2000)$, where the radar is at the origin. Its initial local coordinates are given as $\hat{x}_{target}(0) = \left(0,-1/\sqrt{2},1/\sqrt{2}\right)$, $\hat{y}_{target}(0) = \left(0,-1/\sqrt{2},-1/\sqrt{2}\right)$, and $\hat{z}_{target}(0) = (0,0,1)$. For the scenario 1 and 2, the target moves in a straight and level flight condition toward $\hat{x}_{target}(0)$ direction with a constant velocity, 136m/s. For the scenario3, the target moves in the sustain turn with 5G condition toward $\hat{y}_{target}(t)$ with a constant velocity, 136m/s. The EAD is assumed to be ejected from the target when *t*=0. The initial ejector location and ejector angle of the EAD are represented as $\left(x_{l,target}(0), y_{l,target}(0), z_{l,target}(0)\right)$ and $\left(\phi(0),\theta(0),\psi(0)\right)$ in the local coordinates of the target, respectively, where (ϕ,θ,ψ) denotes Euler angles [16].

For the scenarios in Table 3, the linear trajectories of the target and the EAD are calculated as shown in Fig. 8. Fig. 9 shows the angular trajectories of the EAD, $\left(\phi(t),\ \theta(t),\ \psi(t)\right)$

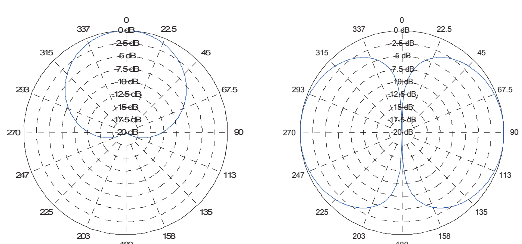

(a) (b)

Fig. 7. Two different beam patterns of EAD. (a) End-fire and (b) Broad-side.

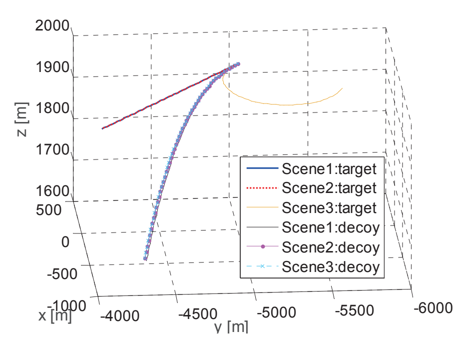

Fig. 8. Linear trajectories of target and EAD on three operation scenarios.

Table 3. Three different operation scenarios in local coordinates of the target

	Scenario1	Scenario2	Scenario3
Target movement	Straight and level flight	Straight and level flight	Sustain turn with 5G
Target velocity [m/s]	136	136	136
Ejector location of EAD [m]	$(-2.47,-1,-1)$	$(-0.47,-1.5,-0.05)$	$(-0.47,-1.5,-0.05)$
Ejector angle of EAD [deg]	$(0^\circ,0^\circ,0^\circ)$	$(0^\circ,0^\circ,20^\circ)$	$(0^\circ,0^\circ,20^\circ)$
Ejection force [N]	870	870	870

for all scenarios in Table 3. The local coordinates of the EAD is expressed with respect to initial local coordinates of the target, $\left(\hat{x}_{\text{target}}(0), \hat{y}_{\text{target}}(0), \hat{z}_{\text{target}}(0)\right)$ as

$$\begin{bmatrix} \hat{z}_{\text{EAD}}(t) \\ \hat{y}_{\text{EAD}}(t) \\ \hat{x}_{\text{EAD}}(t) \end{bmatrix} = \begin{bmatrix} 1 & 0 & 0 \\ 0 & \cos\phi(t) & \sin\phi(t) \\ 0 & -\sin\phi(t) & \cos\phi(t) \end{bmatrix} \begin{bmatrix} \cos\theta(t) & 0 & -\sin\theta(t) \\ 0 & 1 & 0 \\ \sin\theta(t) & 0 & \cos\theta(t) \end{bmatrix} \begin{bmatrix} \cos\psi(t) & \sin\psi(t) & 0 \\ -\sin\psi(t) & \cos\psi(t) & 0 \\ 0 & 0 & 1 \end{bmatrix} \begin{bmatrix} \hat{x}_{\text{target}}(0) \\ \hat{y}_{\text{target}}(0) \\ \hat{z}_{\text{target}}(0) \end{bmatrix} \quad (15)$$

The analytical results of the angular trajectories of the EAD in Fig. 9 are under an ideal condition where both the ejector angle and the ejector force are assumed to be constant. Hence, we allow some random deviation (perturbation) of the EAD within 3 degrees from the calculated mean values of ϕ, θ and ψ on the all scenarios for the next Monte Carlo simulations.

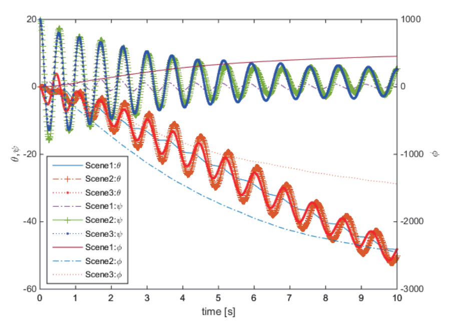

Fig. 9. Angular trajectories of EAD on three operation scenarios.

The results for the scenario 1 are shown in Fig. 10.The proposed numerical scheme can simulate the tracking operation of the radar in accurate fashion based on the estimated time domain echo signal. Fig. 10 (a) shows the received power at the tracking radar from the EAD and the target as a function of time based on the movements of the target and the EAD. The internal amp gain of the EAD is assumed as 45dB with the h-polarization excitation. The perturbation can affect the direction of the antenna beam of the tracking radar, which can vary the received signal level from the EAD. For the scenarios, the simulation time is assumed as 10 sec, during which the tracking radar operates on the circular scan mode to search a target in large area and on the conical scan mode to track the target as described in subsection 2.5. Fig. 10 (b) is the comparison of the trajectories of the target and the EAD, and the estimated trajectories of the beam of the tracking radar. In the global coordinates, the estimated azimuth and elevation angles at the tracking radar are shown in Fig. 10 (c) and (d). To simulate the jamming effect of the EAD, we conduct a Monte Carlo simulation with varying the internal amp gain of the EAD. For every Monte Carlo simulation, 1000 realizations are conducted with varying the direction perturbation of the EAD. Fig. 11 shows the probability of missing target, P_M as a function of the amp gain of the EAD for two different beam patterns. Here, P_M is

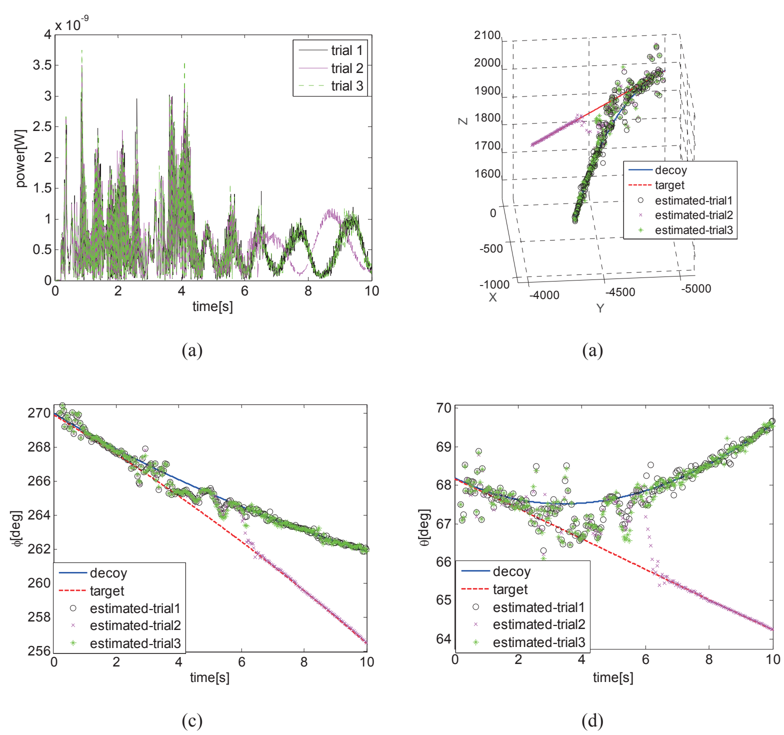

Fig. 10. Received Power of tracking radar and trajectories of target and EAD at three trials for end-fire beam pattern with G_{amp}=45dB and h-pol. on scenario 1. (a) Received Power, (b) Trajectories in global coordinates, (c) Azimuth angle in global coordinates, and (d) Elevation angle in global coordinates.

defined as P_M=1-P_d where P_d is the detection probability of the target. For the scenario 1, to guarantee the survivability of the target, more than 46dB internal power amp gain for the h-polarization and more than 48dB power amp gain for the circular polarization are required for the end-fire beam pattern. When the EAD uses the broad-side beam pattern, at least 41dB power amp gain for the h-polarization and 45dB power amp gain for the circular polarization is demanded for the effective jamming on the scenario 1. The broad-side beam type EAD can provide a better jamming performance than the end-fire beam type EAD on the scenario 1 as the transmitted wave from the radar to EAD is locally off from the bore-sight of the EAD and thus the broad-side beam type EAD has higher antenna gain to the radar. On the other hand, the end-fire beam type EAD can provide much more effective jamming with approximately 40 dB amp gain on both the scenario 2 and the scenario 3, while the broad-side beam type EAD has relatively low antenna gain as the local incident angle is not highly deviated from the bore-sight.

The simulation results for all three different scenarios are summarized in Table 4. Table 4 shows the required power amp gain of EAD for the probability of missing target to be 0.5. i.e. P_M=0.5 on the three scenarios.

4. Conclusion

To design an efficient EAD that maximizes the survivability of a target, a simulator that can calculate the radar echo signals at the tracking radar in the time domain may be required since it is not easy to achieve the same objective based on real experiments. Hence, a method of simulating the received signals at the tracking radar is proposed based on the analysis of target scattering properties and the EAD jamming power calculation by applying the Friis transmission formula. The proposed algorithm considers some important parameters that critically affect the jamming performance of the EAD, such as the movements of the target and the EAD, the antenna pattern, antenna gain, amp gain, the polarizations of the EAD and the tracking radar, and the searching and tracking operations of the radar. The trajectories of the EAD are accurately analyzed by solving 6 DOF equations of motion for the EAD. The proposed algorithm is verified for a simple scenario, where the received

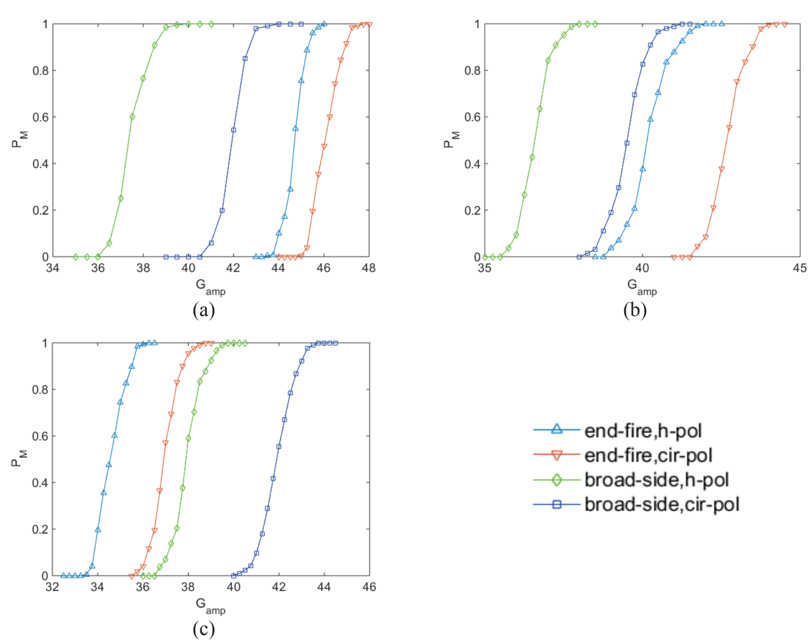

Fig. 11. Probability of missing target P_M as function of internal amp gain of EAD for two different beam patterns. (a) Scenario 1, (b) Scenario 2, and (c) Scenario 3.

Table 4. Required power amp gain of the EAD for P_M=0.5 on the three scenarios.

	End-fire, h-pol	End-fire, cir-pol	Broad-side, h-pol	Broad-side, cir-pol
Scenario1	44.7 dB	46.14 dB	37.36 dB	41.92 dB
Scenario2	40.19 dB	42.68 dB	39.55 dB	36.63 dB
Scenario3	34.56 dB	36.94 dB	37.88 dB	41.9 dB

power can be analytically calculated. For realistic scenarios, it is numerically shown that the implemented scheme can correctly track the object that returns more power to the radar between two targets. For an application, we assess the jamming performance of two EADs whose antenna patterns and the power amp gains are different. The probability of missing the target is calculated based on the Monte Carlo simulation for three different deployment scenarios. Based on the performance comparison of the different EADs, we can design an efficient EAD guarantying to maximize the survivability of the target.

Acknowledgement

The authors gratefully acknowledge the support from the Electronic Warfare Research Center at Gwangju Institute of Science and Technology (GIST), originally funded by Defense Acquisition Program Administration (DAPA) and the Agency for Defense Development (ADD).

References

[1] F. Neri, *Introduction to Electronic Defense Systems*, Artech House, London, 1991.

[2] D.K. Barton, *Radar Evaluation Handbook*, Artech House, London,1991.

[3] N.B. Benton, "Fiber optic microwave link applications in towed decoy electronic countermeasure systems", *Proceeding of SPIE-The International Society for Optical Engineering*, Bellingham, WA, USA, 1995, pp. 85-92.

[4] W.X. Bai, A.F. Li, and S.B. Li, "Simulation and analysis of radar decoy jamming", *Electronic Information Warfare Technology*, Vol.23, No.4, pp. 53-57, 2008.

[5] F.N. Dr, "Anti-monopulse jamming techniques", *Proceeding of the 2011 SBMO/IEEE MTT-S International Microwave and Optoelectronics Conference*, Belem, Brazil, 2001, pp. 45-50.

[6] D. Curtis Schleher, *Electronic Warfare in the Information Age*, Artech House, MA, USA, 1999.

[7] Kwak, E., Shin, J., Lee, S., Choi, K., Hyun, J. and Kim, N., "Development of an Off-line 6-DOF Simulation Program for Store Separation Analysis", J. *of the Korean Society for Aeronautical and Space Sciences*, Vol. 37, No. 12, 2009, pp. 1252-1257. DOI: 10.5139/JKSAS.2009.37.12.1252.

[8] F. Obelleiro, J. L. Rodriguez, and R. J. Burkholder, "An iterative physical optics approach for anlyzing the electromagnetic scattering by large open-ended cavities", *IEEE Trans. Antennas Propagat.*,Vol. 43, No. 4, 1995, pp. 356-361.

[9] R. J. Bulkholder, C. Tokgoz, C. J. Reddy, and P. H. Pathak, "Iterative Physical Optics: Its not just for cavities anymore", *Proc. IEEE Antennas and Propag. Soc. Int. Symp.*, Vol. 1A, pp. 18-21, 2005.

[10] R. J. Bulkholder, "Forward-backward iterative physical optics algorithm for computing the RCS of open-ended cavities", *IEEE Trans. Antennas Propagat.*, Vol. 53, No. 2, 2005, pp. 793-799.

[11] R.J. Marks II, *Introduction to Shannon Sampling and Interpolation Theory*, Spinger-Verlag, 1991.

[12] Kihwan Jung, Il Suek Koh, and Seungho Choi, "Comparison of Accuracy of Interpolation Methods for Scattered Field of Large Objects: Sinc and VSH (Vector Spherical Harmonics) Functions", *Journal of Korean Institute of Electromagnetic Engineering and Science*, Vol. 2, No.1, 2014.

[13] Balanis, *Antenna Theory*, Wiley-Interscience, 2005

[14] David L. Adamy, *Introduction to Electronic Warfare Modeling and Simulation*, Artech House, 2002.

[15] Merrill Skolnik, *Radar Handbook*, McGraw-Hill, 2007.

[16] Gregory G Slabaugh, *Computing Euler angles from a rotation matrix*, Retrieved on August, 1999.